6.3 Shock Wave Impinging on a Boundary Layer

When a shock wave impinges on a boundary layer it imposes a large adverse pressure gradient. This pressure gradient causes the boundary layer to thicken, and if the shock is sufficiently strong, separation will occur. Shock induced separation can lead to unsteady flow phenomena; the position of the shock may oscillate causing large pressure fluctuations along the surface upon which the boundary layer is growing. This type of behaviour has an important bearing on the design of control surfaces for supersonic aircraft. Consequently, the study of shock induced separation has in the past received much attention through experimentation. With the development of CFD it is now possible to study such phenomena using numerical simulation. But before a CFD code can be used in earnest it must be carefully validated. To this end, many workers have computed the stylized shock/boundary layer problem that was studied experimentally by Hakkinen *et al*[30]; an oblique shock wave impinges on the laminar boundary layer which grows over a flat plate. Note, for this problem the flow does not oscillate and so a steady-state solution is sought. Although many acceptable sets of results have been obtained for the pressure and skin friction profiles along the plate, for example[19, 38, 63], it has been argued that this state of affairs is just fortuitous. For the resolution of these calculations was insufficient to resolve all the salient features of the flow. Indeed for some calculations the width of the incident shock was comparable to the width of the separation bubble! Therefore, a failure to resolve the correct amount of viscous diffusion could be masked by the large amount of numerical diffusion present in these calculations. Using a Navier-Stokes solver[4]in conjunction with the AMR algorithm we have been able to resolve all the salient features of the flow.

6.3.1 Calculation Details

Several different cases were studied by Hakkinen *et al*, we chose to compute the case for which the Reynolds number is given as 2.96×10^5. Note, this Reynolds number is based on free stream conditions and the length from the leading edge of the plate to the point of impingement. In common with most of the simulations for this problem, our calculation assumed that viscosity varies with temperature in accordance with Sutherland's law. Unfortunately, this introduces an element of uncertainty into the calculation. For, Sutherland's law requires the free stream temperature, see equation B.13, but the experimental value for T_∞ is not given by Hakkinen *et al*. So, we have assumed that the wind tunnel reservoir was in thermal equilibrium with ambient conditions. Thus, taking $T_{o_\infty} \approx 288K$ and given M_∞ as 2.0 we estimate $T_\infty \approx 160K$.

The grid G_o was formed from a single uniform mesh of 60 by 20 cells. A further three grid levels were controlled by the automatic grid adaption process. The various

[4]A brief description of this solver is given in appendix B.

parameters used by the adaption process are tabulated in figure 6.21. This table also indicates the monitor function used by the flagging for refinement process. In addition to the usual function based on density gradients, we employed an analogous function based on shear stresses.

With reference to figure 6.22, the following boundary procedures were applied: along the inflow boundary, AB, free stream conditions were specified taking M_∞ as 2.0; along the outflow boundary, CD, extrapolation from the interior was employed; along the plate, LD, an adiabatic no-slip procedure was applied; ahead of the plate, AL, a reflection boundary procedure was used; along the top of the flow domain, BC, extrapolation from the interior was employed, except for the point B where post-shock values where specified in order to generate the incident shock with $\phi = 32.6^o$.

l	rI_l	rJ_l	$Ftol_l$	$Ptol_l$	Monitor Function
0	N/A	N/A	0.05	0.6	Density + Shear Stress
1	4	4	0.05	0.6	Density + Shear Stress
2	2	4	0.15	0.6	Shear Stress
3	2	4	N/A	N/A	N/A

Figure 6.21: Parameters used to control the adaption process for the shock/boundary layer calculation.

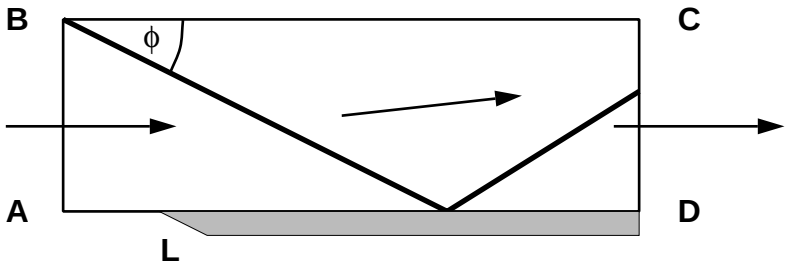

Figure 6.22: Sketch of the numerical domain for the shock/boundary layer calculation.

6.3.2 Results

Figure 6.23 shows a sketch of the salient features for this shock/boundary layer problem. The impinging shock wave causes the boundary layer to thicken and form a bump containing a separation bubble. On the windward side of this bump a compression fan is formed to turn the flow in on itself. This fan eventually coalesces to form the 1^{st} reflected shock. Behind the compression fan, an expansion fan is formed to turn the flow over the crest of the bump. After this expansion fan the flow is once more turned in on itself and another

compression fan forms. This fan coalesces to form the 2^{nd} reflected shock. Additionally, at the leading edge of the plate a weak shock wave is formed as the flow is compressed by the front of the boundary layer. Density contours[5] for our numerical solution are shown in figure 6.26, and the corresponding computational grid is shown in figure 6.27. All the salient features of the flow are easily identified. So, qualitatively at least, our numerical solution is excellent.

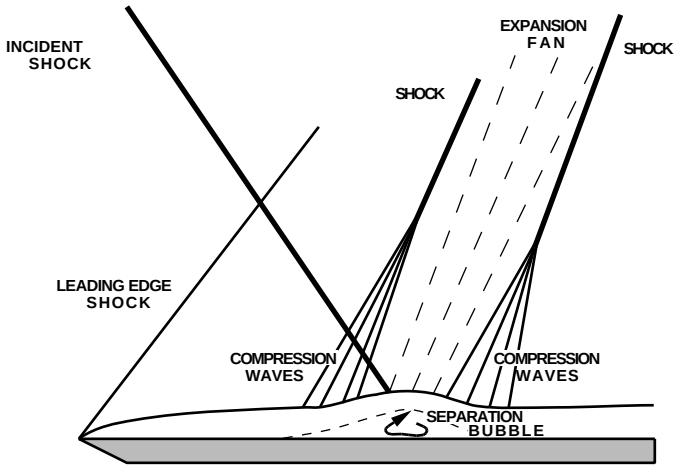

Figure 6.23: Salient flow features for a shock wave impinging on a boundary layer.

A quantitative comparison between our calculation and experiment for the pressure profile along the surface of the plate is given in figure 6.24. The general agreement is good, and would appear to be within the bounds set by the uncertainty in the experimental measurements. Indeed, nothing conclusive may be deduced from the small discrepancies between the two profiles. The experiment also measured values of skin friction along the surface of the plate, and a comparison between these measurements and values calculated from our numerical solution is given in figure 6.25. But the usefulness of this comparison is doubtful. Firstly, skin friction measurements were not taken in the separated region. Secondly, the accuracy of those measurements that were taken has been questioned[2]. Values for skin friction were obtained using a Preston tube which had been calibrated in the absence of a pressure gradient. Therefore, in the presence of an adverse pressure gradient this method of measurement is likely to yield values of skin friction which are higher than the true values. This observation has been used to explain the fact that all the published numerical results for this test problem predict the point of zero skin friction to be upstream of that measured using the Preston tube. Our numerical results are consistent with this line of reasoning. Finally, it should be noted that our numerical results for skin friction correlate more closely with other numerical results than they do with experiment.

[5] 40 contours drawn at 2.5% intervals.

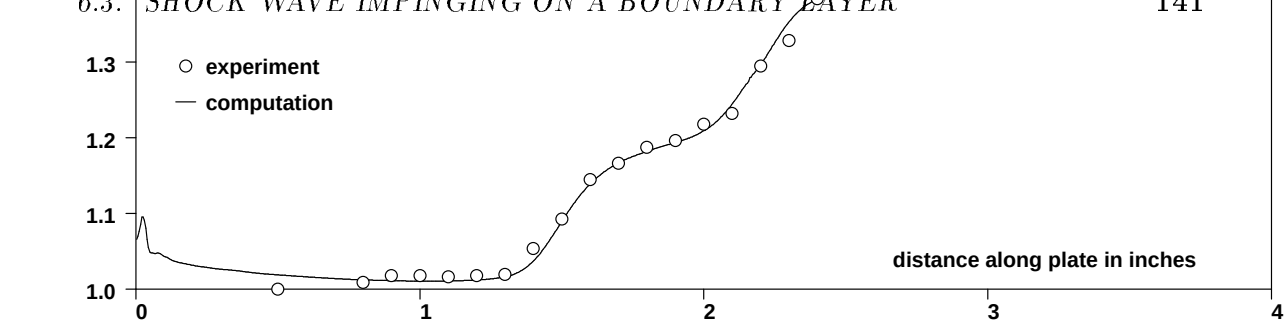

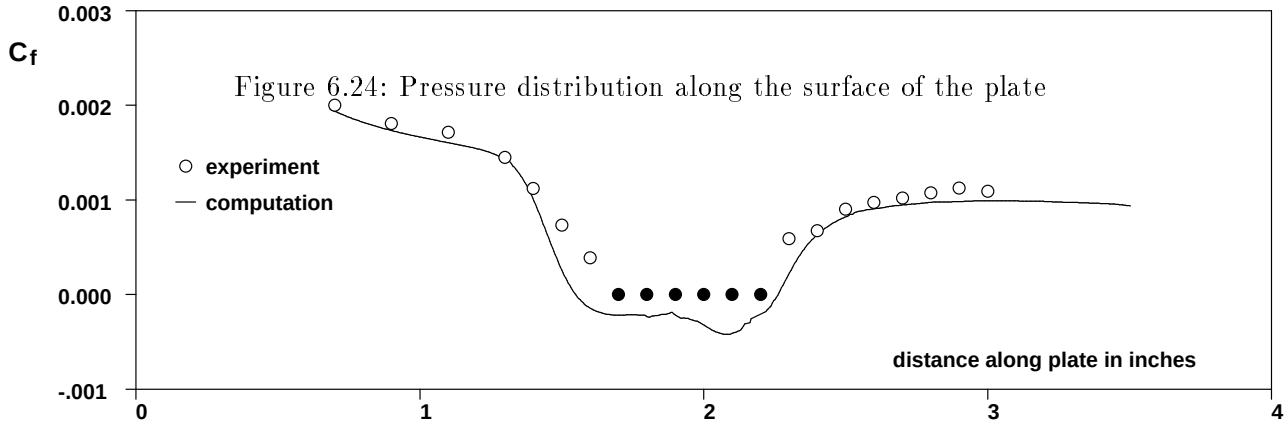

Figure 6.24: Pressure distribution along the surface of the plate

Figure 6.25: Skin-friction distribution along the surface of the plate

6.3.3 Comment

With hindsight, this experiment does not make a particularly good test problem with which to validate a CFD code, because it does not allow a conclusive quantitative comparison to be made. This is not a criticism of the experiment. Indeed, the experiment was performed in the late 1950s, and so the purpose to which the results would be put in the 1990s could not be foreseen. We have included this test problem because of its popularity, and because it highlights many of the difficulties of validating a CFD code.

Although the AMR algorithm has been designed with the aim of simulating transient flows, as this section shows, it is also able to compute solutions to steady flows. But in its current form the algorithm is not particularly suited to such calculations. The flow solution is simply marched to a steady solution in a time accurate manner. Consequently, the rate of convergence is very slow. Indeed, the present calculation took approximately seven days to converge. But many schemes which are quite quick to converge cannot employ local mesh refinement. So, despite its slow convergence rate, the AMR algorithm might prove attractive for studying steady-state problems where the resolution of the solution is paramount. Finally we note, given the hierarchical nature of our grid system, it would be a relatively simple matter to incorporate standard multigrid operators[41] into the flow integration process. In principle this would significantly increase the rate of convergence. Therefore the AMR algorithm could well form the basis for an efficient tool with which to study steady flow problems.

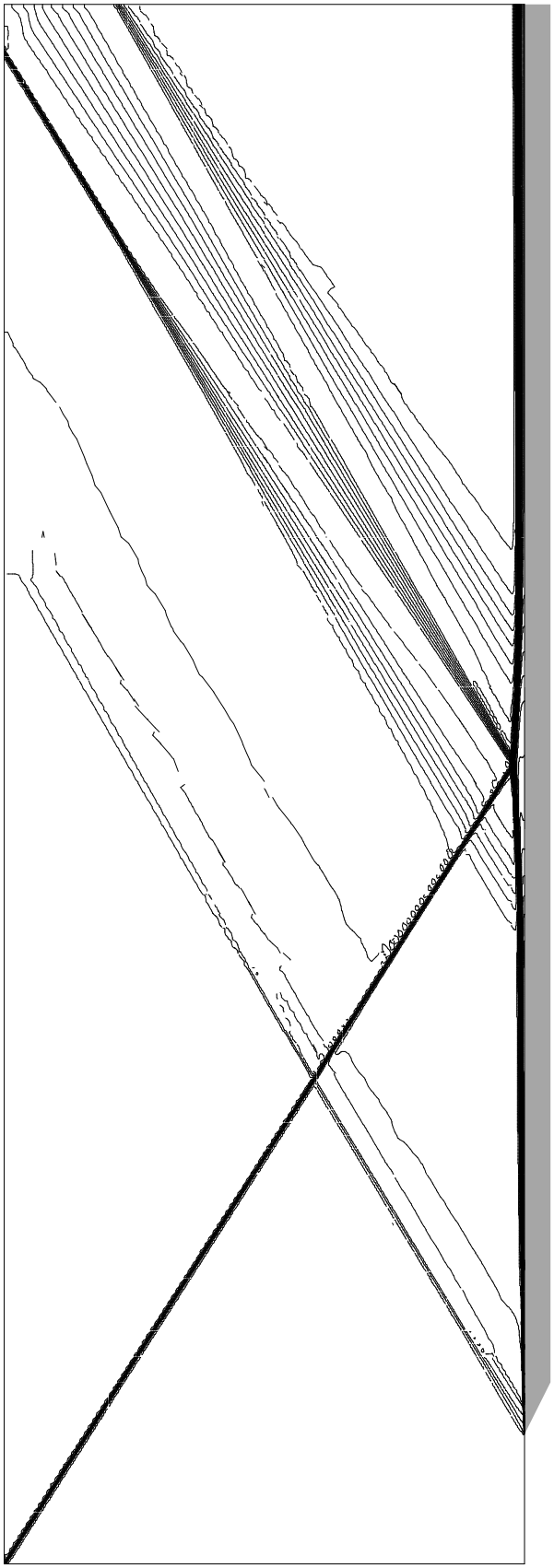

Figure 6.26: Density contours for shock/boundary layer test problem.

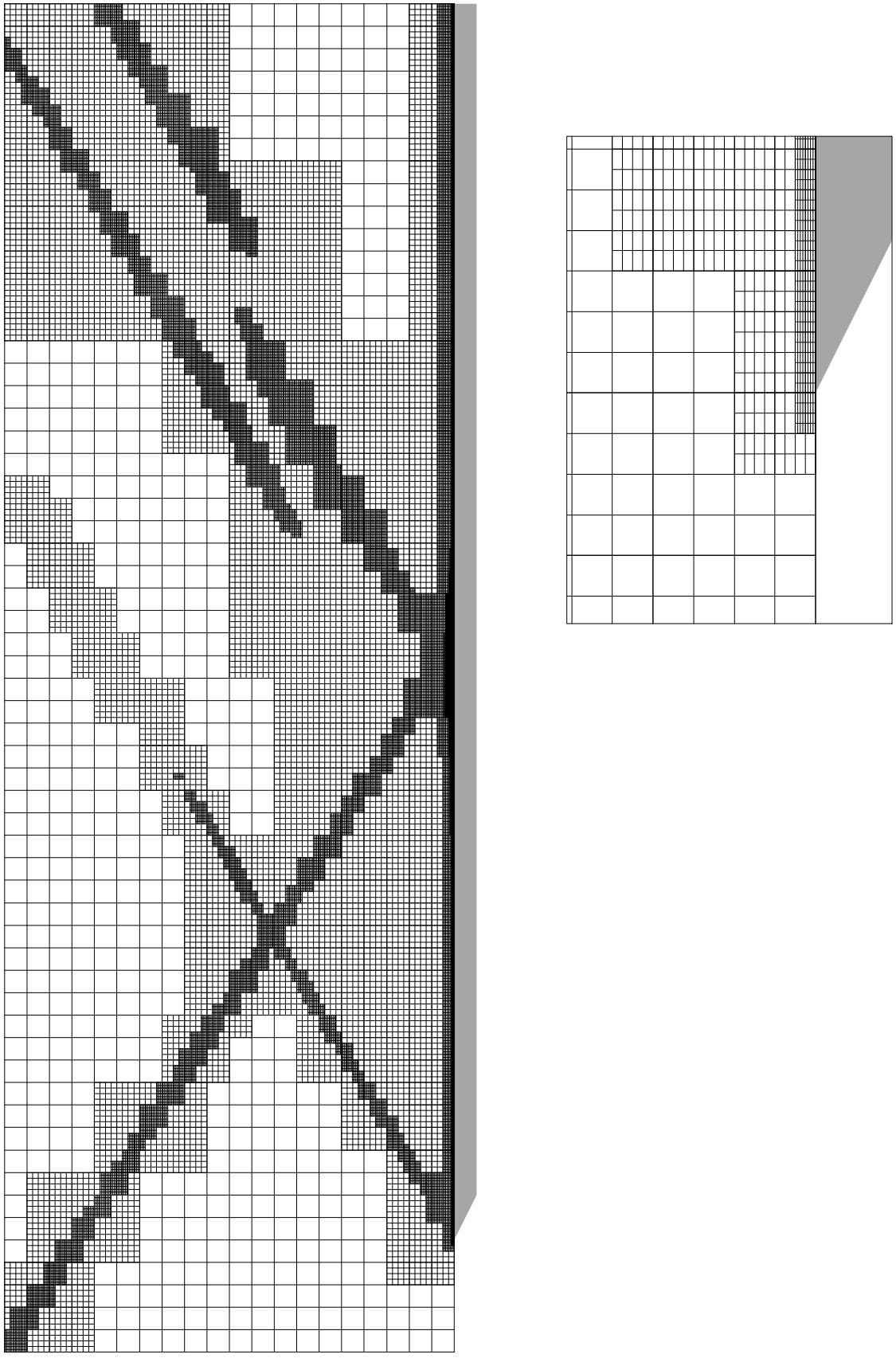

Figure 6.27: Computational grid corresponding to contours shown in figure 6.26.

6.4 Closing Comment

The results presented in this chapter amply demonstrate the worth of the AMR algorithm for simulating shock hydrodynamic flows. Nevertheless, there are features of the algorithm that could be improved upon. But, in view of the difficulties we have experienced in attempting to validate our code, the standard test problems beloved by CFD algorithm developers are likely to be inadequate for the purposes of assessing any notional improvements which might be made. Firstly, those test problems which allow conclusive assessments to be made are for simple flows. Therefore there is no guarantee that any improvement will in fact carry through to the sorts of problem that are of genuine interest. So, using such tests it will be difficult to determine which modifications to the algorithm are significant and which are not. Secondly, the more realistic test problems are generally taken from dated experiments which by today's standards used poor experimental techniques. Therefore as our validation process has shown, these tests rarely allow conclusive quantitative assessments to be made. But the introduction of a new set of test problems based upon more recent experiments would not necessarily improve matters.

From the algorithm developer's point of view, a good validation test should be able to distinguish between the vagaries of the physical model and the vagaries of the numerical method. Consequently, unless an experiment is performed with the express intention of validating a numerical simulation its worth to the algorithm developer is likely to be small. For example, many schemes which are used to simulate viscous flows assume a thin shear layer model. This is done in order to improve computational efficiency. Now, such a model will not be correct for separated flows. However, it may be tolerable for flows containing regions of mildly separated flow. To see if this is the case some workers have simulated Hakkinen's shock/boundary layer experiment. But this experiment does not provide values of skin-friction in the separated flow region, the one region in which the physical model is questionable. So the experiment is useless for the purpose of determining the validity of a thin shear layer model for mildly separated flows.

The need to design experiments to validate CFD codes has been recognized by Glaz *et al*[28], and they have built up an impressive collection of interferograms for shock reflection type problems. As yet, this approach is not widely appreciated. But we believe such collaborative ventures are essential if the accuracy of today's simulations is to be significantly improved upon. To develop the AMR algorithm further we would like reliable experimental results which could provide full flowfield information for a variety of test problems, each problem having been designed to check a specific feature of the algorithm. Since it is inevitable that compromises would have to be struck between what is desirable computationally and what is attainable experimentally, such a set of test problems could only be designed in conjunction with an experimental group.